PLOS ONE

RESEARCH ARTICLE

Towards non-invasive characterisation of coronary stent re-endothelialisation – An in-vitro, electrical impedance study

Ian Holland*, Christopher McCormick, Patricia Connolly

Department of Biomedical Engineering, University of Strathclyde, Glasgow, Scotland, United Kingdom

* ian.holland@strath.ac.uk

Check for updates

OPEN ACCESS

Citation: Holland I, McCormick C, Connolly P (2018) Towards non-invasive characterisation of coronary stent re-endothelialisation – An in-vitro, electrical impedance study. PLoS ONE 13(11): e0206758. https://doi.org/10.1371/journal.pone.0206758

Editor: Masuko Ushio-Fukai, Medical Collge of Gerogia at Augusta University, UNITED STATES

Received: June 25, 2018

Accepted: October 18, 2018

Published: November 5, 2018

Copyright: © 2018 Holland et al. This is an open access article distributed under the terms of the Creative Commons Attribution License, which permits unrestricted use, distribution, and reproduction in any medium, provided the original author and source are credited.

Data Availability Statement: All relevant data are within the paper and its Supporting Information files.

Funding: This work has been funded by the Engineering and Phyiscal Sciences Research Council (www.epsrc.ac.uk, grant number: EP/F50036X/1) as part of an Engineering Doctorate. The funders had no role in study design, data collection and analysis, decision to publish, or preparation of the manuscript.

Abstract

The permanent implantation of a stent has become the most common method for ameliorating coronary artery narrowing arising from atherosclerosis. Following the procedure, optimal arterial wall healing is characterised by the complete regrowth of an Endothelial Cell monolayer over the exposed stent surface and surrounding tissue, thereby reducing the risk of thrombosis. However, excessive proliferation of Smooth Muscle Cells, within the artery wall can lead to unwanted renarrowing of the vessel lumen. Current imaging techniques are unable to adequately identify re-endothelialisation, and it has previously been reported that the stent itself could be used as an electrode in combination with electrical impedance spectroscopic techniques to monitor the post-stenting recovery phase. The utility of such a device will be determined by its ability to characterise between vascular cell types. Here we present *in-vitro* impedance spectroscopy measurements of pulmonary artery porcine Endothelial Cells, Human Umbilical Vein Endothelial Cells and coronary artery porcine Smooth Muscle Cells grown to confluence over platinum black electrodes in clinically relevant populations. These measurements were obtained, using a bespoke impedance spectroscopy system that autonomously performed impedance sweeps in the 1kHz to 100kHz frequency range. Analysis of the reactance component of impedance revealed distinct frequency dependent profiles for each cell type with post confluence reactance declines in Endothelial Cell populations that have not been previously reported. Such profiles provide a means of non-invasively characterising between the cell types and give an indication that impedance spectroscopic techniques may enable the non-invasive characterisation of the arterial response to stent placement.

Introduction

Coronary artery disease is a leading cause of morbidity throughout Europe and worldwide [1]. The growth of an atherosclerotic lesion within an artery occludes blood flow and provides a site for thrombus formation. Treatment of the disease has progressed significantly over the recent decades and has been greatly aided by the development of an array of amelioratory intervention procedures of which coronary stent implantation can be considered one of the

Competing interests: PC discloses interest in intellectual property described in: A system and method for cell characterisation. World intellectual property organisation. WO 2009/GB01132, 2009 plus EP2271933 and US2011144469. This does not alter our adherence to PLOS ONE policies on sharing data and materials.

most successful. Since their first reported use in 1986 [2], coronary stents have moved through several phases of development, from first generation, bare metal versions to current modern drug eluting-devices [3].

Improvements in stent design have been driven by the need to reduce the post procedural occurrences of In-Stent Restenosis (ISR) and thrombosis. ISR is classified through angiography as a 50% reduction in the diameter of the artery in the region of stent implantation, through neointimal cell proliferation, inhibiting blood flow and endangering the life of the patient [4–6]. It is a consequence of damage to the arterial wall caused by stent expansion. The resulting inflammatory response to this vascular injury is a complex cascade mechanism that ultimately results in the proliferation of Smooth Muscle Cells (SMCs) over the stent struts. The advent of a class of stents with an anti-proliferative drug-eluting coating significantly reduced ISR occurrence and the most extensively used stents now present with ISR rates of around 3–4%, per year [7,8]. More recently neoatherosclerosis, the reoccurrence of lipid laden lesions, has been also been identified as an additional, later stage stent failure mode [9,10].

The optimal course of cellular regrowth following stent implantation is the reformation of a complete monolayer of functional endothelial cells (ECs) forming a barrier between the implant surface and the circulating blood [11,12]. Uncovered, exposed stent surfaces increase the risk of platelet activation, initiation of the coagulation cascade and the dangerous scenario of thrombus development [12]. To reduce the risk of thrombus formation, prolonged anti-platelet drug regimens are common. However, these come with an increased risk of bleeding and are not be suitable for all patients, particularly those with comorbidities [13,14]. With endothelialisation complete, withdrawal of anti-platelet therapy can be considered, however there are still no clinically available means of assessing the extent of EC proliferation over the stent struts. Current diagnostic techniques such as angiography, Magnetic Resonance Imaging and Computed Tomography have insufficient resolutions, as well as the presence of stent induced artefacts [15,16]. Consequently, these methods are unable to determine the status of the EC layer. Imaging modalities, such as optical coherence tomography and intravascular ultrasound, delivered to the stent region by catheterisation, can provide more detailed images showing cellular regrowth but are also limited in resolution and their invasive nature precludes routine use. Methods of non-invasively monitoring successful re-endothelialisation may address this limitation [17,18], and reveal wider insights into the mechanisms driving ISR and neoatherosclerosis.

A self-reporting stent, capable of providing temporal data on the vascular response to stent injury has been proposed, whereby the conductive properties of a metallic stent are exploited to carry out electrical impedance spectroscopic measurements to monitor cellular regrowth [18]. The concept of remotely monitoring neointimal growth in this way has been explored using mathematical modelling [19], an ex-vivo model [18], in-vivo balloon mounted electrodes [20], and patent activity in this area indicating possible future commercial developments [21,22]. The closest technological embodiment to this concept has been achieved by Oxley et al with an impedance-based stent, termed Stentrode. The device comprised a modified endovascular stent with platinum disk electrodes that recorded impedance variation via percutaneous leads that were implanted into sheep cerebral veins. The group identified an increase in capacitance that was attributed to neointimal growth [23,24]. However, the groups focus in developing such a device was as a step towards the recording and stimulation of neural activity and the vascular cells responsible for this impedance behaviour were not determined. Given the quite different roles that endothelial and smooth muscle cells play in clinical outcomes following stenting described above, it is therefore important to determine if impedance spectroscopy can non-invasively characterise between the vascular cell types associated with ISR and reendothelialization.

In-vitro use of impedance spectroscopy has been extensively used to non-invasively gain insights into a wide range of cellular behaviours such as micromotion [25], mitochondrial dysfunction [26], stem cell differentiation [27–29] and EC barrier function [30,31]. This research has been greatly facilitated by the availability of commercial impedance systems such as Applied Biophysics, ECIS system and ACEA Biosciences xCELLigence range. However, these systems feature small electrode geometries and are limited by the available frequency range resolution, with the xCELLigence system constrained to measurements at one of only 3 frequencies [31]. Cellular regrowth such as re-endothelialisation occurs over a range of exposed strut areas of 10-100mm2, several orders of magnitude greater than the micro scale electrodes commonly used in impedance studies. For the purposes of addressing the feasibility of a self-reporting stent to determine re-endothelialisation the electrode should be of a comparable size to capture data from a clinically relevant cell population.

Impedance measurements have previously been shown to be able to characterise different cell types in the determination of stem cell differentiation into osteogenic [27], adipogenic [28], neuronal [32] and cardiomyocyte [33] lineages. Haas et al, also demonstrated that the switching of rat aortic SMCs from a proliferative to a quiescent phenotype could be determined by reductions in total impedance measured across a 1kHz to 1MHz range [34]. Rümenapp et al, also reported distinct total impedance ratio variations across the same frequency range when investigating the effect of drug toxicity on murine fibroblasts [35]. We therefore hypothesised that impedance measurements in the high frequency kilohertz range would enable non-invasive characterisation between different vascular cell types as they proliferate to confluence.

To achieve the dual aims of wide frequency range measurement on stent comparable vascular cell populations we constructed a bespoke system capable of autonomously capturing impedance data in a physiologically relevant environment. Here we present the use of the developed system to carry out, impedance measurements of the primary vascular cell types pulmonary artery porcine endothelial cells, Human Umbilical Vein Endothelial Cells (HUVECs) and coronary artery porcine smooth muscle cells, as they proliferate to confluence.

Materials and methods

Cell culture chambers

Gold electrodes were evaporated onto Falcon 35mm diameter petri dish [36] surfaces using the laser cut mask pattern shown in Fig 1. Compression of a 4.2cm2 culture cube (Lab-Tek chamber slide, Nunc, USA) onto the dish surface sealed a cell culture area containing a large reference electrode (100mm2) and an array of 4 smaller working electrodes (each 7mm2). Electrodes were galvanostatically coated with platinum black (36mA/cm2 for 1.5 seconds) in a 2 electrode setup with a platinum wire anode in platinising solution (0.06M Chloroplatinic acid hexahydrate and 794μM of lead acetate in deionised water, both, Sigma-Aldrich, Poole, United Kingdom) using a Solartron SI-1287 Electrochemical interface (Solartron Analytical, Farnborough, United Kingdom).

Impedance measurement system

Impedance measurements at 50mV excitation voltage in the frequency range 1kHz to 100kHz were taken at a temporal resolution of 2 hours using a bespoke automated impedance system developed for this study. This allowed all measurements to be taken without removal of the cell culture chambers from the incubator. The system comprised an Autolab PGSTAT302N, (Metrohm, Herisau, Switzerland) with automated switching between 8 individual chambers performed using a 32 channel multiplexer (Analog devices, Norwood, Massachusetts, United

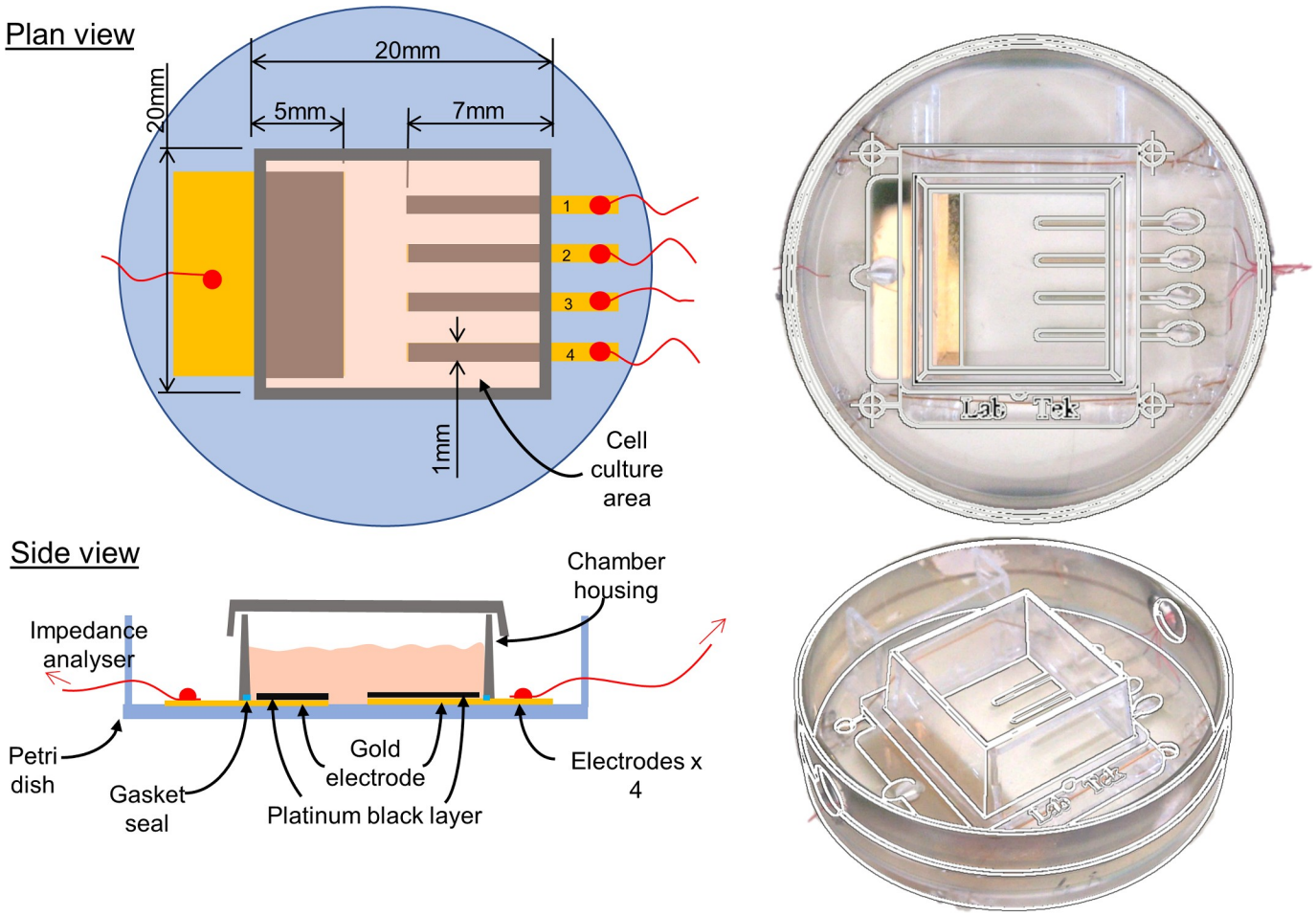

Fig 1. Chamber design with cell culture surface and electrode arrangement.

https://doi.org/10.1371/journal.pone.0206758.g001

States) controlled via an Arduino 2560 development board and a bespoke LabView program (National Instruments, Texas, United States). Impedance sweep data were logged as text files before chronological ordering and importation into Microsoft excel software.

Cell culture

Primary ECs were isolated from the pulmonary arteries of pig hearts obtained fresh from a local abattoir. A scalpel blade was gently scraped across the luminal surface of a section of the pulmonary artery proximal to the heart. The cells were then suspended and cultured in Medium 200 with 2% Low Serum Growth Supplement (Invitrogen, Paisley, Scotland) and 1% penicillin–streptomycin (Sigma-Aldrich, Poole, United Kingdom). Primary SMCs were isolated from the left anterior descending coronary artery (LAD) from the same hearts, based on a previously optimised laboratory explant method [37]. Briefly, a 3cm section of the proximal LAD was dissected out from the heart and cut free from surrounding fat and connective tissue. The artery was then sectioned into 3mm length rings, which were transferred to cell culture flasks (2 rings per 25 cm2) containing 50:50 Waymouth's MB752/1 and F-12 Nutrient Mixture (Ham) (Invitrogen), 10% FBS (European source) and 1% penicillin–streptomycin. The artery rings were removed from the culture flask once it was clear that a viable population of cells with an SMC morphology had grown out from the artery and adhered to the culture surface.

Typically, this took place around 10 days following the initial incubation. HUVECs, (Lonza, Basel, Switzerland, No. CC-2517) were grown in endothelial cell growth medium EGM2 BulletKit media (Lonza). All cell types were cultured in a humified atmosphere at 37˚C (5% CO2/ 95% air). For impedance experiments cells were seeded into chambers at passages 2 to 4 at sub confluent densities to allow proliferation to confluence to be measured and observed. ECs were seeded into chambers in the density range 4.5–6.5 x 104 cells cm-2, SMCs 2.5–3.125 x 104 cells cm-2, HUVECs 4.125–5.1 x 104 cells cm-2, with no cells seeded into control chambers. Media was replaced every 48 hours in all chambers.

Light microscopy

Electrodes were sufficiently transparent to permit imaging using an inverted light microscope (Motic, China) and cell growth to confluency was observed, with chambers removed from the incubator and images captured every 24 hours.

Immunofluorescence

The primary porcine cell line isolation procedure was characterised initially with light microscopy observation of EC and SMC morphologies and subsequently through immunofluorescence imaging of paraformaldehyde fixed cells using Von Willebrand Factor (VWF) (1:400, Abcam, Cambridge, United Kingdom) for ECs and α Smooth Muscle Actin (αSMA) (1:400, Sigma-Aldrich,) for SMCs. Nuclei were stained with 4',6-diamidine-2-phenylindole (DAPI) (1μg/ml, Sigma-Aldrich). Negative controls were performed by staining ECs for αSMA and SMCs for VWF. Fluorescent microscopy images were captured using a Zeiss Axio Imager Z1 (Cambridge, United Kingdom).

Data presentation

For each cell type and control, impedance data were collated from electrodes and a mean calculated for each frequency at a given time point in the experiment. No cell-electrode circuit model was used to further process data presented in this paper. The maximum Standard Error Mean (SEM) is stated in the figure caption where error bars are not visible at the scales used. Three-dimensional representation of impedance data variation with time and frequency was carried out using dedicated LabView software.

Results

Immunofluorescence

Successful isolation and establishment of EC and SMC lines was confirmed with immunofluorescence and light microscopy imaging. ECs in culture displayed the typical cobblestone morphology that is a well-established feature for this cell type [38,39] (Fig 2A) and expressed the endothelial cell marker VWF (Fig 2C). SMCs in culture displayed the elongated spindle morphology typical of smooth muscle cells [40] (Fig 2B) and expressed the smooth muscle cell marker αSMA (Fig 2D). Negative controls of ECs stained with αSMA showed no expression (Fig 2E). SMCs stained for VWF expression exhibited minimal staining indicating that a low level of ECs may be present in the isolated cell population as previously reported for SMC isolation protocols [41] (Fig 2F).

Electrode platinisation

Impedance measurements were taken of bare gold electrodes in EC media before and after the addition of the thin film platinum black coating. Fig 3 shows that the addition of the platinum

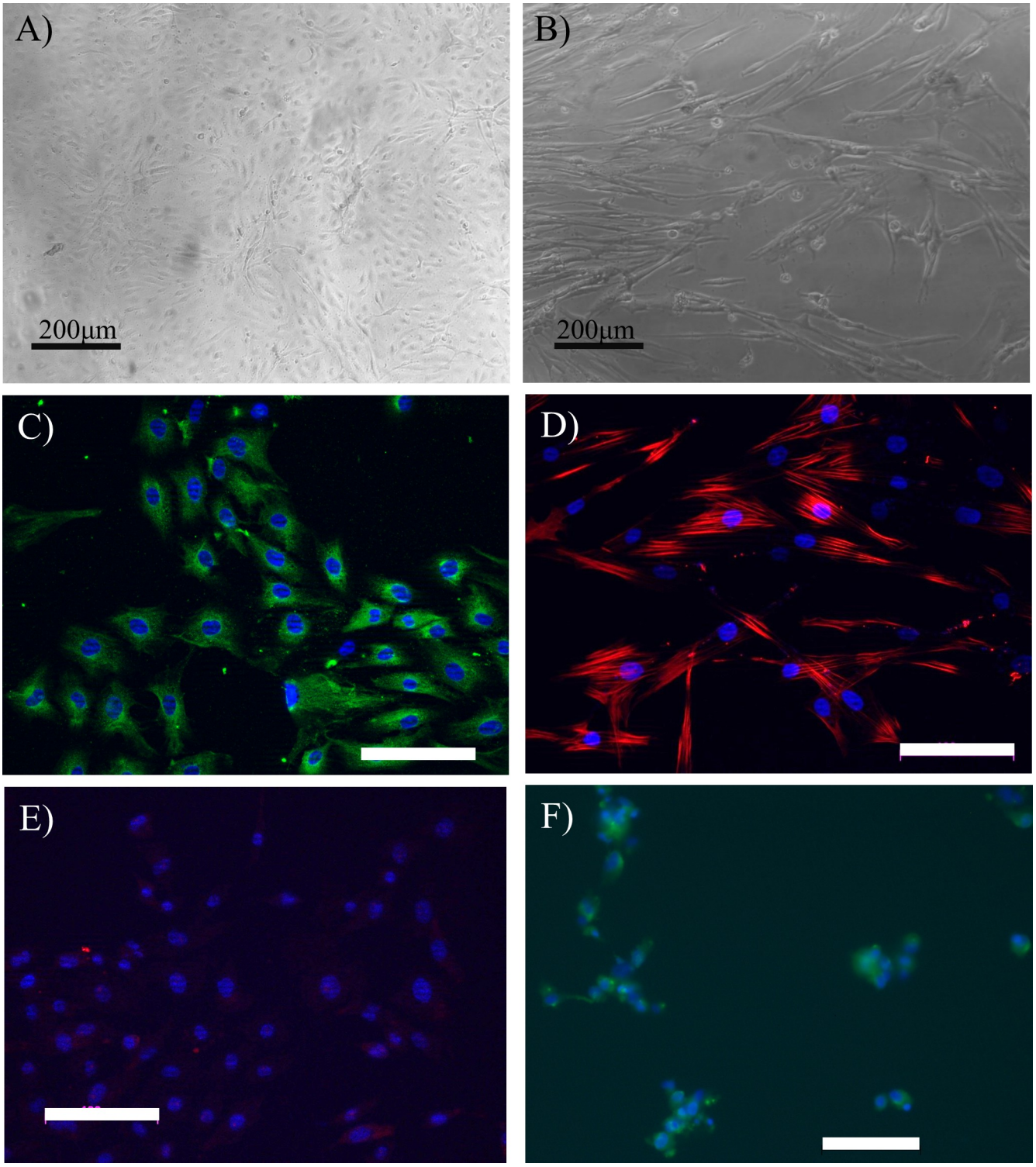

Fig 2. Primary cell isolation light microscopy and immunofluorescence characterisation. Light microscopy images showing typical morphologies for (A) isolated ECs and (B) SMCs. (C) ECs positively stained for the marker Von Willebrand factor (green). (D) Smooth muscle cells positively stained for alpha smooth muscle actin (red). (E) Negative control, ECs showing minimal staining for alpha smooth muscle actin (red). (F) Negative control, SMCs showing minimal staining for Von Willebrand factor (green). Images were taken of cells at passage 2. White scale bars are 100μm, all nuclei stained with DAPI (blue).

https://doi.org/10.1371/journal.pone.0206758.g002

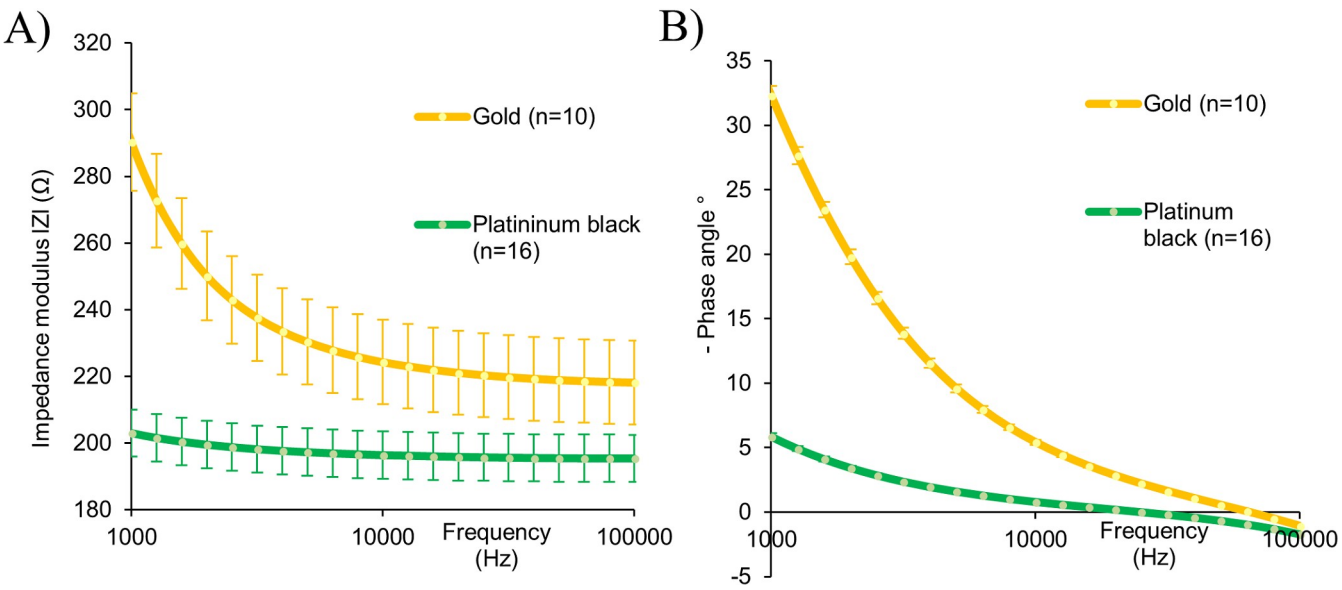

Fig 3. Impedance spectra of gold and platinised electrodes. (A) Impedance modulus and (B) phase angle. Data captured in EC media and represent the mean ± SEM (gold n = 10, platinum n = 16). Error bars are not visible for phase measurements at the scale used, max gold SEM 0.771˚ and max platinum black SEM 1.076˚.

https://doi.org/10.1371/journal.pone.0206758.g003

black layer coating achieved a reduction in total impedance (|Z|) and phase angle when compared to the gold substrate alone.

Cell characterisation impedance measurements

A previously used method for monitoring cell monolayers using impedance is the total impedance normalised ratio, calculated by dividing the total impedance of a cell covered electrode at the beginning of the experiment with the total impedance of the same cell free electrode at the beginning of the experiment, defined in Eq 1 [21,35,42].

$$Total\ impedance\ normalised\ ratio = \frac{|Z|_{Cell\ covered\ electrode}}{|Z|_{Cell\ free\ electrode}} \quad (1)$$

Mean electrode data using this ratio from the three cell types tested is displayed in Fig 4 along with the same ratio for media only cell free control electrodes. Porcine ECs (Fig 4A) and HUVECs (Fig 4B) displayed a similar trend of elevating values as confluence increased, with HUVECs exhibiting greater magnitudes. SMCs showed an initial decline in total impedance ratio that climbed towards cell free electrode values as they attained confluence, however cell seeded electrodes did not show large deviations from cell free control electrodes (Fig 4C).

The capacitive reactance component of impedance has previously been used to monitor cell proliferation over electrodes [27,36,43,44]. Reactance data at electrodes seeded with the 3 vascular cell types is displayed in Fig 5, at the frequency of 10kHz, the median of the frequency range used in this study and a commonly used frequency for analysis in cellular impedance studies [31,34,45,46]. To highlight impedance variation arising from the effect of cellular proliferation reactance values were normalised by subtraction from the first values recorded immediately after cell seeding or media addition. Normalisation of impedance values in this fashion enables comparison with data sets reported in other impedance studies [34,47,48], and is also applied to measurements made using commercially available systems [31]. Also shown in Fig 5 are light microscopy images of representative electrode tips, showing cell proliferation

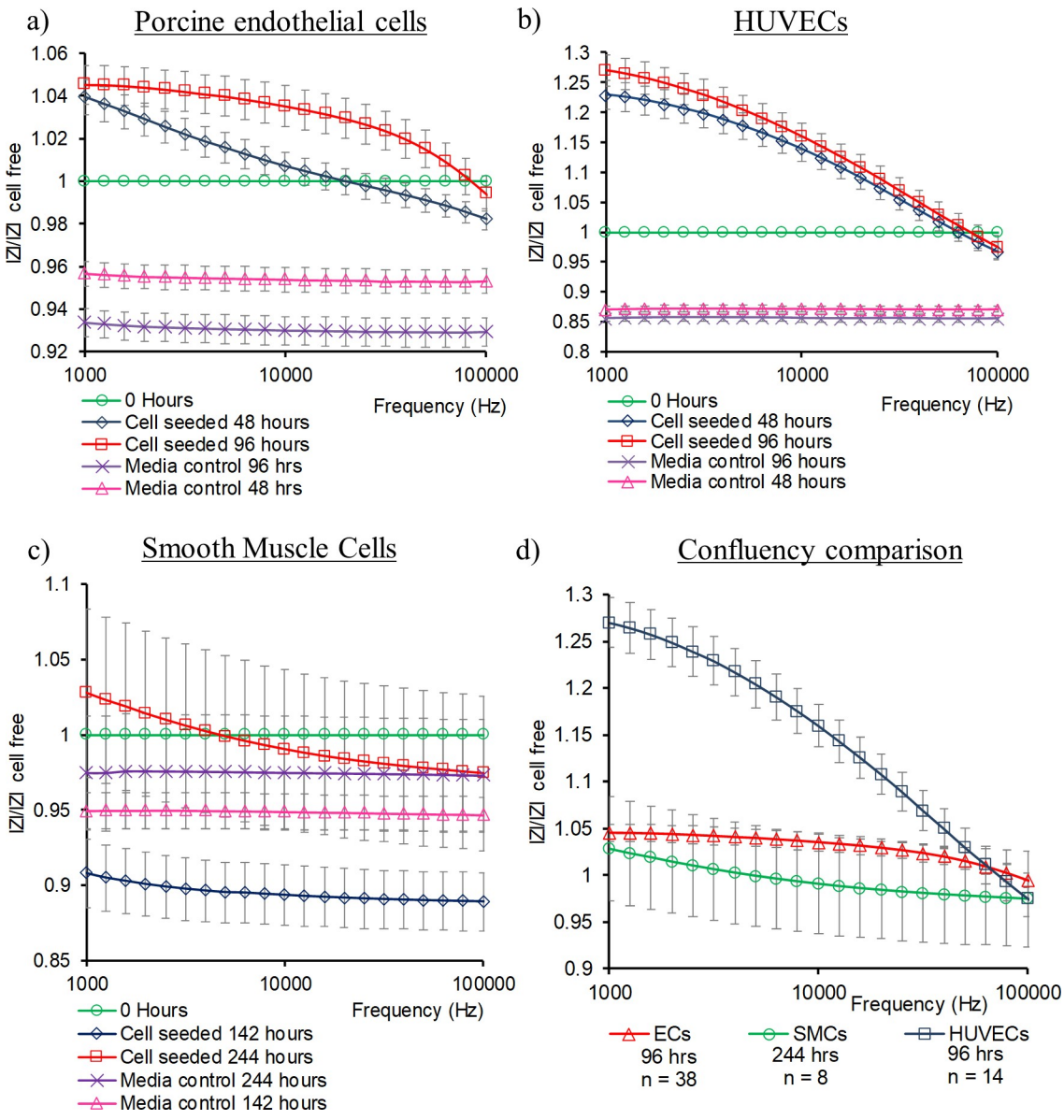

Fig 4. Mean total impedance ratio for confluent monolayers. (A) porcine ECs (n = 38) and media control electrodes (n = 33), (B) HUVECs (n = 14) and media control electrodes (n = 10), (C) SMCs (n = 8), and media control electrodes (n = 8), (D) Cell comparison at confluence. Error bars are ± SEM.

https://doi.org/10.1371/journal.pone.0206758.g004

to confluence. Microscopy observations showed that SMCs took longer to attain confluence than ECs, consistent with the slower rise in reactance observed for SMCs compared to ECs. All cell types exhibited a climb in reactance as cells first settled and then proliferated over the electrodes correlating with light microscopy observations. Minimal reactance variation was seen in control chambers containing media only. Following observation of confluence, ECs and HUVECs demonstrated a reduction in reactance magnitude (Fig 5A and 5E). Such a post confluence decline was not evident in the SMC data (Fig 5I). HUVECs demonstrated a similar reactance profile in comparison to ECs but with elevated magnitudes, 7 times higher at peak values (Fig 5E).

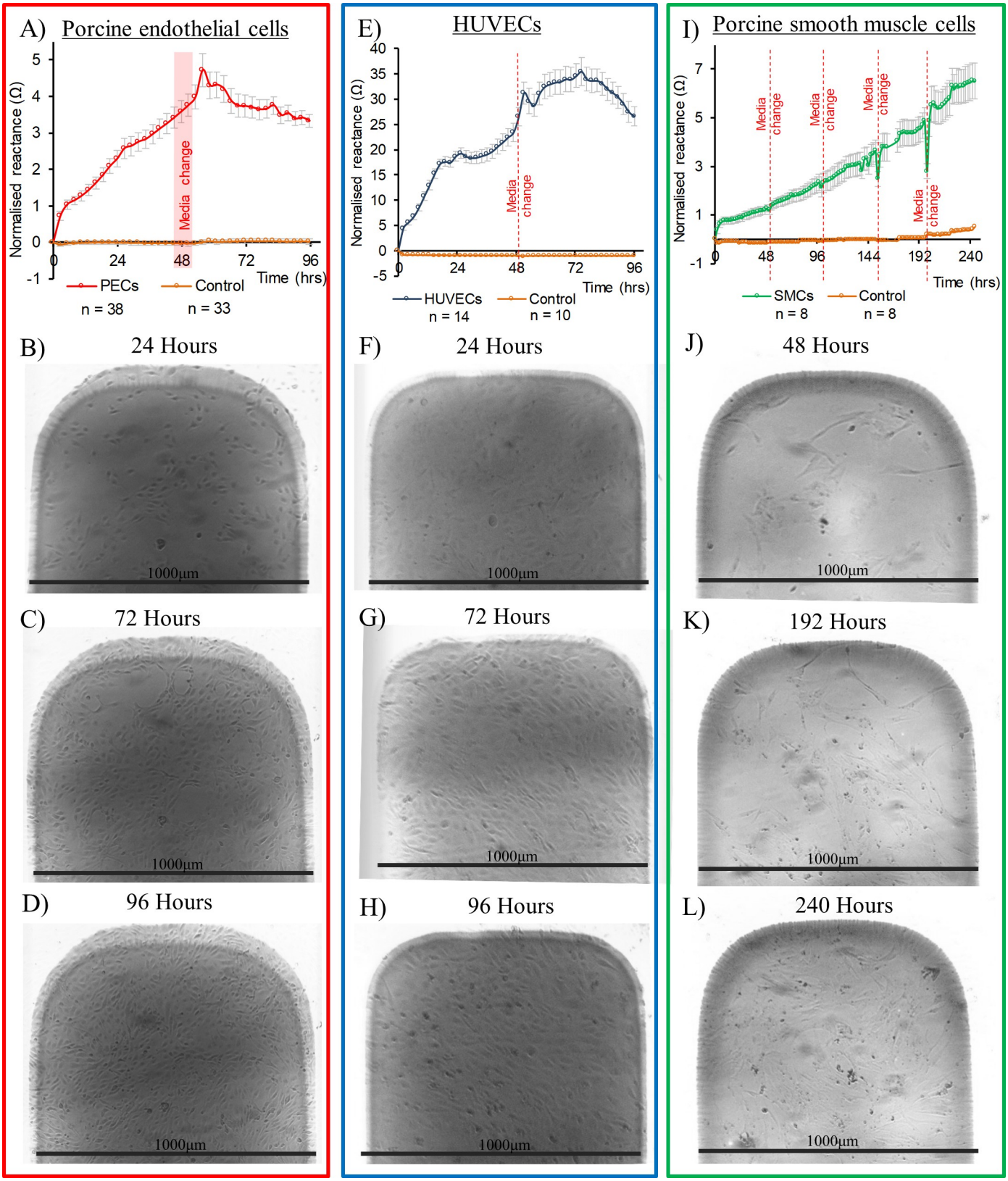

Fig 5. Reactance profiles at 10kHz and corresponding representative light microscopy images. Light microscopy images for Porcine ECs (B) to (D), HUVECs (F) to (H) and SMCs (J) to (L). Black scale bars are provided by known electrode width of 1000µm. Mean reactance profiles at 10kHz for cell seeded and cell free electrodes (A) Porcine ECs, (E) HUVECs and (I) SMCs. Red lines represent media changes. Error bars are ± SEM.

https://doi.org/10.1371/journal.pone.0206758.g005

3D presentation of impedance variation in both time and frequency data has been demonstrated as an effective method to portray frequency dependent impedance data captured from cell monolayers [49–51]. Mean reactance data in the frequency range 1kHz to 100kHz, from the 3 vascular cell types is presented in Fig 6. ECs reactance displayed a complex pattern with peaks occurring earlier towards the lower 1kHz end of the spectrum and delayed at higher frequencies towards 100kHz (Fig 6A). HUVEC reactance was found to be maximal when measured at 30kHz after 72 hours of culture (Fig 6C). SMCs showed no reactance decreases at any of the measured frequencies (Fig 6E). Control electrodes are shown at the same scale as the corresponding cell covered electrodes and demonstrated minimal change in reactance over the measurement period (Fig 6B, 6D and 6F). 3D presentation of mean total impedance is available in supporting information S1 Fig.

Discussion

The non-invasive monitoring of cellular regrowth in the post-stenting recovery phase has the potential to reveal insights into the progression of vascular diseases such as thrombosis, in-stent restenosis and neoatherosclerosis. Impedance spectroscopy is increasingly being used to monitor various aspects of cell function, although its application within the study of vascular pathologies has been more limited. To our knowledge, it has not been applied to characterise the vascular cell types that play important roles in such pathologies. To enable label-free characterisation of vascular cells, we developed an in-vitro impedance spectroscopy system to carry out continuous automated measurements in populations comparable to those seen covering implanted stents.

The addition of a platinum black coating to the electrodes used in the system reduced their overall impedance and is comparable to published data for platinum black electrodes [52]. Such impedance reductions from plain metal thin film electrodes can be attributed to an increased surface area for current flow owing to the coatings increased roughness, and improve sensitivity to impedance changes arising from cellular adhesion [53,54].

The total impedance ratio, previously used to identify motility [42] and cell detachment [35], here revealed distinct profiles for the three cell types examined. The total impedance of a monolayer can be correlated with its ability to form a selective boundary between its apical and basolateral sides, also termed its barrier function [30,31,55]. It is the formation of junctions between cells that contribute to its barrier function. SMCs do not form monolayer barriers in-vivo and with none of the tight junction complexes seen in endothelial cells [56], resulting in a comparably lower total impedance ratio on confluence. In the context of total impedance measurements taken of neointimal growth, reduced values may indicate a partially covered implant surface or a prevalence of non-barrier forming cell types such as SMCs.

Greater distinction between the vascular cell types was observed through 3D representation of the reactance component of impedance. Each reactance profile for 3 cell types, HUVECs, porcine endothelial and smooth muscle cells exhibited different characteristics and provides a potential method of non-invasively characterising these cell types. The elevation in reactance seen in all cell types as they proliferate over the electrode surface corresponds with similar studies involving impedance spectroscopy measurements of cell monolayers, with frequency (f) dependent reactance (Z") typically converted into capacitance (C) according to the equation $C = 1/2\pi fZ''$ [57]. The reactance of a cell is determined by the capacitive effect of the cell membrane and various organelles within [57,58]. The shape and arrangements of these organelles and membranes are matched to each cell's specific functionality and it is therefore reasonable to assume that capacitive reactance measurements of these elements of the cell will reveal differences between cell types [26,59], as presented here. It is acknowledged that impedance

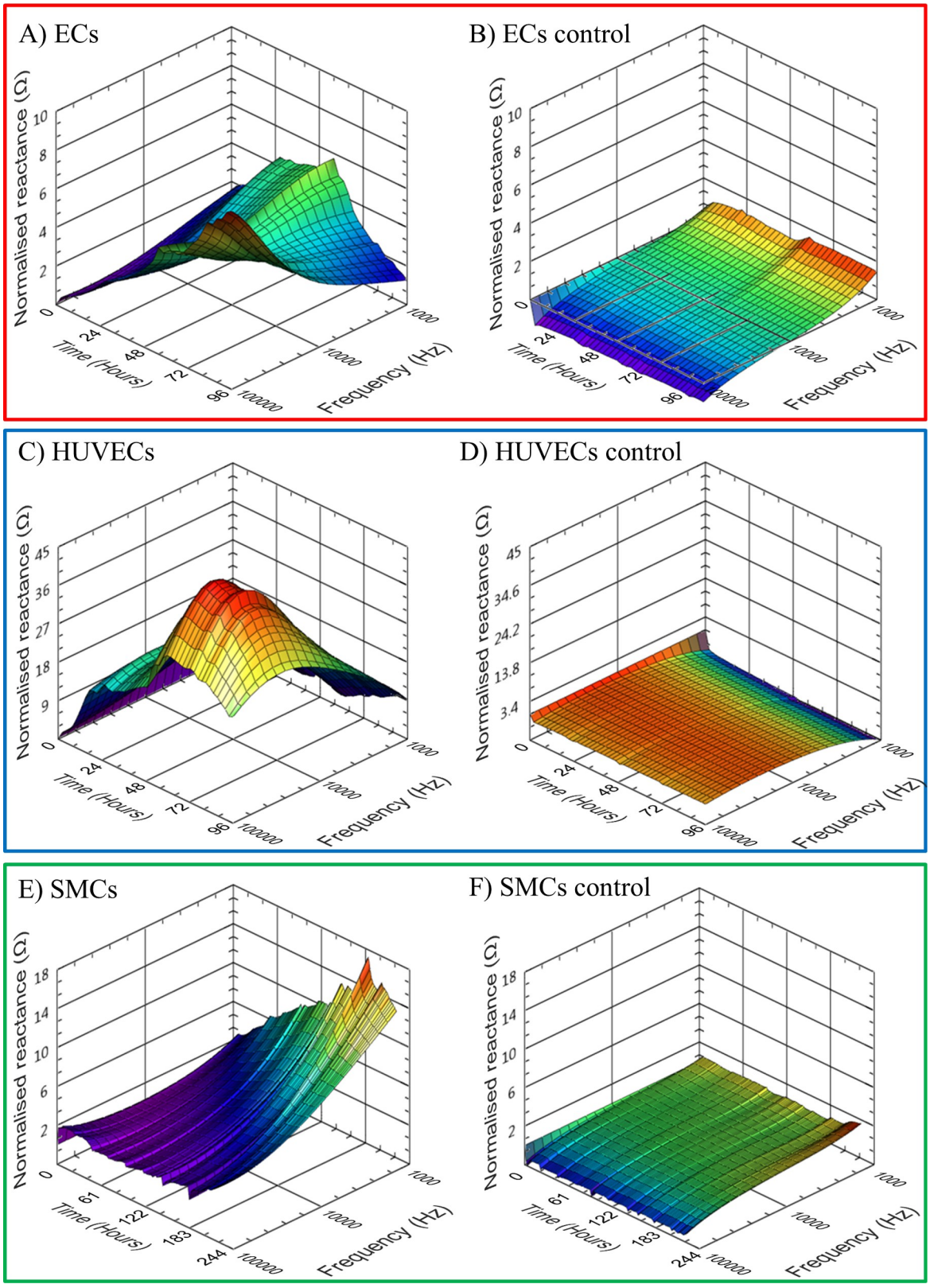

Fig 6. Mean electrode 3D normalised reactance profiles for duration of culture. (A) ECs n = 38, max SEM = 0.908, (B) EC control, n = 33, max SEM = 0.405, (C) HUVECs, n = 14, max SEM = 3.354, (D) HUVEC control, n = 10, max SEM = 1.054, (E) SMCs n = 8, max SEM = 1.861 and (F) SMC control, n = 8, max SEM = 0.778.

https://doi.org/10.1371/journal.pone.0206758.g006

measured across a frequency range will report results from different regions of a cell monolayer, with the current path at low frequencies bypassing the cell membrane and measuring the paracellular space whilst higher frequencies are transcellular, through the cells interior [43,58,60,61]. By measuring over a frequency range that includes elements of paracellular and transcellular current pathways, the results presented here capture a spectrum of data throughout the different cell type monolayers that enables characteristic reactance profiles to be elucidated. The observed variation in reactance peaks between porcine aortic ECs and HUVECs provides evidence that the technique may be sufficiently sensitive to provide a means of characterisation between cell phenotypes, additional experimentation, with a wider variety of cell types, is required to further validate this proposal.

Post confluence declines in reactance were measured in the EC and HUVEC data with maximal falls of 78% and 32% respectively. However, these large reactance declines occurred with no corresponding change in microscopy observed cell morphology or cell death events. Total impedance and capacitive reactance reductions have been previously reported to correspond with induced cell death from cytotoxic agonists [62] and confluence related contact inhibition [63]. Non-death related events too can cause significant changes such as cell junction related barrier function modulation [30,31] and linage differentiation [27]. The observed reactance decline in confluent endothelial cell populations could be attributable to cell monolayer maturation processes such as cytoskeletal bound junction formation [64] and extra cellular matrix deposition [65]. Further experimentation will be required to investigate these hypotheses.

Our results show that simplified in-vitro models of the post-stenting regrowth scenarios of re-endothelialisation and ISR can be non-invasively characterised using impedance spectroscopic techniques. In the envisaged in-vivo environment cell regrowth patterns will occur over complex stent electrode geometries alongside pulsatile blood flow and it may be necessary to develop an electrode–cell model to simplify and elucidate the key impedance markers of cell specific proliferation. Such a model may also be useful in enabling clinicians to interpret impedance data. The translation of this in-vitro experimentation towards a self-reporting stent for use in a clinical environment as previously proposed [18,19] is however a considerable technological challenge. The electrical circuitry miniaturisation needed to fit inside an artery without occluding blood flow and non-contact transmission of data without the need for percutaneous leads represents a step change in current implanted electrical device design. Current miniaturisation of impedance devices for implantation is best represented in the 13mm diameter device developed by Rodriguez et al [66]. The most immediate use for the technology is therefore likely to be in the research domain with the development of an in-vivo research tool to help provide greater insights from the animal models that are widely used in this research field [67]. Such a device could capture data, in real-time, of cardiovascular disease progression, providing insights that help inform the development of advanced stents in the future.

The disease states of restenosis, in stent thrombosis and the optimal re-endothelialisation process take place in a complex, in-vivo, 3D environment comprising interaction with multiple cell types and pulsatile blood flow, in contrast to the 2D static single cell culture conditions described here. Further study in physiological flow conditions are therefore required in order to fully assess the potential of this technology. Intriguingly, it has previously been shown that endothelial cells in flow conditions exhibit increases in transendothelial resistance [68], suggesting that the cell specific impedance data presented here may be accentuated in in-vivo conditions. A further consideration is that in an in-vivo environment both smooth muscle cells and endothelial cells may proliferate over the stent struts, a scenario not included in our experiments. A co-culture model of smooth muscle cells with an upper layer of endothelial cells [69,70] would reveal further insights into the capabilities of impedance spectroscopy to

characterise post-stenting cell regrowth. An additional limitation of the present study is the use of primary porcine cells. Whilst pigs can be considered as a good model for human cardiovascular disease and are used in a large array of cardiovascular studies [8,71,72] greater clinical relevance could be obtained through the use of primary human, coronary artery cells.

In summary the results show that analysis of the reactance component of impedance, if captured over a sufficiently wide frequency range, can provide a method of comparatively characterising vascular cells. This affirms the non-invasive characterisation capabilities of impedance spectroscopy previously demonstrated for other cell types when determining stem cell differentiation. Future work will aim to further examine vascular cell impedance properties via the monitoring of their respective differentiation processes.

Supporting information

S1 File. Impedance data set.
(XLSX)

S1 Fig. Mean electrode 3D normalised total impedance profiles for duration of culture. (A) ECs n = 38, max SEM = 2.96, (B) EC control, n = 33, max SEM = 1.54, (C) HUVECs, n = 14, max SEM = 6.79, (D) HUVEC control, n = 10, max SEM = 4.99, (E) SMCs n = 8, max SEM = 26.53 and (F) SMC control, n = 8, max SEM = 9.65.
(TIF)

Acknowledgments

Porcine hearts were kindly donated by Robertson's Fine Foods, (Ardrossan, Scotland). HUVECs were kindly provided by Claire McCluskey and Dr Susan Currie of the Strathclyde Institute of Pharmacy & Biomedical Sciences.

Author Contributions

Conceptualization: Ian Holland, Christopher McCormick, Patricia Connolly.

Data curation: Ian Holland.

Formal analysis: Ian Holland, Christopher McCormick, Patricia Connolly.

Funding acquisition: Patricia Connolly.

Investigation: Ian Holland.

Methodology: Ian Holland, Christopher McCormick, Patricia Connolly.

Project administration: Christopher McCormick, Patricia Connolly.

Resources: Christopher McCormick, Patricia Connolly.

Software: Ian Holland.

Supervision: Christopher McCormick, Patricia Connolly.

Validation: Ian Holland.

Visualization: Ian Holland.

Writing – original draft: Ian Holland.

Writing – review & editing: Christopher McCormick, Patricia Connolly.

References

1. Nichols M, Townsend N, Luengo-Fernandez R, Leal J, Gray A, Scarborough P, et al. European cardiovascular disease statistics 2012. European Heart Network. 2012.
2. Sigwart U, Puel J, Mirkovitch V, Joffre F, Kappenberger L. Intravascular Stents to Prevent Occlusion and Re-Stenosis after Transluminal Angioplasty. N Engl J Med. 1987. https://doi.org/10.1056/NEJM198703193161201 PMID: 2950322
3. O'Brien B, Zafar H, Ibrahim A, Zafar J, Sharif F. Coronary Stent Materials and Coatings: A Technology and Performance Update. Ann Biomed Eng. 2016; 44(2):523–35. https://doi.org/10.1007/s10439-015-1380-x PMID: 26139297
4. Mitra AK, Agrawal DK. In stent restenosis: bane of the stent era. J Clin Pathol. 2006. https://doi.org/10.1136/jcp.2005.025742 PMID: 16505271
5. Piraino D, Cimino G, Buccheri D, Dendramis G, Andolina G, Cortese B. Recurrent in-stent restenosis, certainty of its origin, uncertainty about treatment. Int J Cardiol. https://doi.org/10.1016/j.ijcard.2016.12.073 PMID: 28038808
6. Stefanini GG, Holmes DR. Drug-Eluting Coronary-Artery Stents. N Engl J Med. 2013. https://doi.org/10.1056/NEJMra1210816 PMID: 23323902
7. Sarno G, Lagerqvist B, Fröbert O, Nilsson J, Olivecrona G, Omerovic E, et al. Lower risk of stent thrombosis and restenosis with unrestricted use of "new-generation" drug-eluting stents: A report from the nationwide Swedish Coronary Angiography and Angioplasty Registry (SCAAR). Eur Heart J. 2012; 33(5):606–13. https://doi.org/10.1093/eurheartj/ehr479 PMID: 22232428
8. Byrne RA, Serruys PW, Baumbach A, Escaned J, Fajadet J, James S, et al. Report of a European Society of Cardiology-European Association of Percutaneous Cardiovascular Interventions task force on the evaluation of coronary stents in Europe: Executive summary. Eur Heart J. 2015; 36(38):2608–20. https://doi.org/10.1093/eurheartj/ehv203 PMID: 26071600
9. Alfonso F, Byrne RA, Rivero F, Kastrati A. Current treatment of in-stent restenosis. J Am Coll Cardiol. 2014; 63(24):2659–73. https://doi.org/10.1016/j.jacc.2014.02.545 PMID: 24632282
10. Park SJ, Kang SJ, Virmani R, Nakano M, Ueda Y. In-stent neoatherosclerosis: A final common pathway of late stent failure. J Am Coll Cardiol. 2012; 59(23):2051–7. https://doi.org/10.1016/j.jacc.2011.10.909 PMID: 22651862
11. Inoue T, Croce K, Morooka T, Sakuma M, Node K, Simon DI. Vascular inflammation and repair: Implications for re-endothelialization, restenosis, and stent thrombosis. JACC Cardiovasc Interv. 2011; 4(10):1057–66. https://doi.org/10.1016/j.jcin.2011.05.025 PMID: 22017929
12. Tesfamariam B. Endothelial Repair and Regeneration Following Intimal Injury. J Cardiovasc Transl Res. 2016; 9(2):91–101. https://doi.org/10.1007/s12265-016-9677-1 PMID: 26797874
13. Finn A V., Nakazawa G, Joner M, Kolodgie FD, Mont EK, Gold HK, et al. Vascular responses to drug eluting stents: Importance of delayed healing. Arterioscler Thromb Vasc Biol. 2007; 27(7):1500–10. https://doi.org/10.1161/ATVBAHA.107.144220 PMID: 17510464
14. Lüscher TF, Steffel J, Eberli FR, Joner M, Nakazawa G, Tanner FC, et al. Drug-eluting stent and coronary thrombosis: Biological mechanisms and clinical implications. Circulation. 2007; 115(8):1051–8. https://doi.org/10.1161/CIRCULATIONAHA.106.675934 PMID: 17325255
15. Andreini D, Pontone G, Mushtaq S, Bartorelli AL, Bertella E, Trabattoni D, et al. Coronary in-stent restenosis: assessment with CT coronary angiography. Radiology. 2012; 265(2):410–7. https://doi.org/10.1148/radiol.12112363 PMID: 22966068
16. van Geuns RJ, Baks T. Magnetic Resonance Imaging for Restenosis. In: Essentials of restenosis for intervential cardiologists. Towta, New Jersey: Humana Press; 2007. p. 277–85.
17. Manoharan G, Davidavicius G, Wijns W. Clinical Presentation of Restenosis. In: Essentials of restenosis for intervential cardiologists. Towta, New Jersey: Humana Press; 2007. p. 29–46.
18. Shedden L, Kennedy S, Wadsworth R, Connolly P. Towards a self-reporting coronary artery stent—measuring neointimal growth associated with in-stent restenosis using electrical impedance techniques. Biosens Bioelectron. 2010; 26(2):661–6. https://doi.org/10.1016/j.bios.2010.06.073 PMID: 20667708
19. Rivas-Marchena D, Olmo A, Miguel J, Martínez M, Huertas G, Yúfera A. Real-Time Electrical Bioimpedance Characterization of Neointimal Tissue for Stent Applications. Sensors. 2017; 17(8):1737.
20. Streitner I, Goldhofer M, Cho S, Kinscherf R, Thielecke H, Borggrefe M, et al. Cellular imaging of human atherosclerotic lesions by intravascular electric impedance spectroscopy. PLoS One. 2012; 7(4):2–6.
21. Shedden L, Connolly P. A system and method for cell characterisation. World intellectual property organisation. WO 2009/GB01132, 2009.

22. Barakat A, Bozsak F, Bonnassieux YE, Le Bruno P, Francais O, Carreel B. Medical device provided with sensors having variable impedance. France: World intellectual property organisation; WO 2016/050972 A1, 2016.
23. Opie NL, John SE, Rind GS, Ronayne SM, Grayden DB, Burkitt AN, et al. Chronic impedance spectroscopy of an endovascular stent-electrode array. J Neural Eng. IOP Publishing; 2016; 13(4).
24. Oxley TJ, Opie NL, John SE, Rind GS, Ronayne SM, Wheeler TL, et al. Minimally invasive endovascular stent-electrode array for high-fidelity, chronic recordings of cortical neural activity. Nat Biotechnol. 2016; 34(3):320–7. https://doi.org/10.1038/nbt.3428 PMID: 26854476
25. Giaever I, Keese CR. Micromotion of mammalian cells measured electrically. Proc Natl Acad Sci U S A. 1991; 88(17):7896–900. PMID: 1881923
26. Padmaraj D, Pande R, Miller JH, Wosik J, Zagozdzon-Wosik W. Mitochondrial membrane studies using impedance spectroscopy with parallel pH monitoring. PLoS One. 2014; 9(7).
27. Bagnaninchi PO, Drummond N. Real-time label-free monitoring of adipose-derived stem cell differentiation with electric cell-substrate impedance sensing. Proc Natl Acad Sci U S A. 2011; 108(16):6462–7. https://doi.org/10.1073/pnas.1018260108 PMID: 21464296
28. Angstmann M, Brinkmann I, Bieback K, Breitkreutz D, Maercker C. Monitoring human mesenchymal stromal cell differentiation by electrochemical impedance sensing. Cytotherapy. 2011; 13(9):1074–89. https://doi.org/10.3109/14653249.2011.584863 PMID: 21619493
29. Öz S, Maercker C, Breiling A. Embryonic carcinoma cells show specific dielectric resistance profiles during induced differentiation. PLoS One. 2013; 8(3):e59895. https://doi.org/10.1371/journal.pone.0059895 PMID: 23533658
30. Szulcek R, Bogaard HJ, van Nieuw Amerongen GP. Electric Cell-substrate Impedance Sensing for the Quantification of Endothelial Proliferation, Barrier Function, and Motility. J Vis Exp. 2014;(85):1–12.
31. Bischoff I, Hornburger MC, Mayer BA, Beyerle A, Wegener J, Fürst R. Pitfalls in assessing microvascular endothelial barrier function: impedance-based devices versus the classic macromolecular tracer assay. Sci Rep. 2016; 6(March):23671. https://doi.org/10.1038/srep23671 PMID: 27025965
32. Lee R, Kim I-S, Han N, Yun S, Park KI, Yoo K-H. Real-time discrimination between proliferation and neuronal and astroglial differentiation of human neural stem cells. Sci Rep. 2014 Jan; 4:6319. https://doi.org/10.1038/srep06319 PMID: 25204726
33. Jahnke H-G, Steel D, Fleischer S, Seidel D, Kurz R, Vinz S, et al. A novel 3D label-free monitoring system of hES-derived cardiomyocyte clusters: a step forward to in vitro cardiotoxicity testing. PLoS One. 2013 Jan; 8(7):e68971. https://doi.org/10.1371/journal.pone.0068971 PMID: 23861955
34. Haas S, Jahnke H-G, Glass M, Azendorf R, Schmidt S, Robitzki A a. Real-time monitoring of relaxation and contractility of smooth muscle cells on a novel biohybrid chip. Lab Chip. 2010; 10(21):2965–71. https://doi.org/10.1039/c0lc00008f PMID: 20835426
35. Rümenapp C, Remm M, Wolf B, Gleich B. Improved method for impedance measurements of mammalian cells. Biosens Bioelectron. 2009; 24(9):2915–9. https://doi.org/10.1016/j.bios.2009.02.030 PMID: 19321331
36. Giaever I, Keese CR. Monitoring fibroblast behavior in tissue culture with an applied electric field. Proc Natl Acad Sci U S A. 1984; 81(12):3761–4. PMID: 6587391
37. McCormick C, Jones RL, Kennedy S, Wadsworth RM. Activation of prostanoid EP receptors by prostacyclin analogues in rabbit iliac artery: Implications for anti-restenotic potential. Eur J Pharmacol. 2010; 641(2–3):160–7. https://doi.org/10.1016/j.ejphar.2010.04.035 PMID: 20450909
38. Bouafsoun A, Othmane A, Jaffrézic-Renault N, Kerkeni A, Thoumire O, Prigent AF, et al. Impedance endothelial cell biosensor for lipopolysaccharide detection. Mater Sci Eng C. 2008; 8(5–6):653–61.
39. Tillman BW, Yazdani SK, Neff LP, Corriere MA, Christ GJ, Soker S, et al. Bioengineered vascular access maintains structural integrity in response to arteriovenous flow and repeated needle puncture. J Vasc Surg. 2012; 56(3):783–93. https://doi.org/10.1016/j.jvs.2012.02.030 PMID: 22917043
40. Sandison ME, Dempster J, McCarron JG. The Transition of Smooth Muscle Cells from a Contractile to a Migratory, Phagocytic Phenotype: Direct Demonstration of Phenotypic Modulation. J Physiol. 2016; 594(21):6189–209. https://doi.org/10.1113/JP272729 PMID: 27393389
41. Sharma AK, Donovan JL, Hagerty JA, Sullivan RR, Edassery SL, Harrington DA, et al. Do current bladder smooth muscle cell isolation procedures result in a homogeneous cell population? Implications for bladder tissue engineering. World J Urol. 2009; 27(5):687–94. https://doi.org/10.1007/s00345-009-0391-3 PMID: 19234706
42. Lind R, Connolly P, Wilkinson CDW, Breckenridge LJ, Dow J. Single cell mobility and adhesion monitoring using extracellular electrodes. Biosens Bioelectron. 1991; 6(4):359–67.
43. Michaelis S, Wegener J, Robelek R. Label-free monitoring of cell-based assays: Combining impedance analysis with SPR for multiparametric cell profiling. Biosens Bioelectron. 2013; 49(15):63–70.

44. Cho S, Thielecke H. Electrical characterization of human mesenchymal stem cell growth on microelectrode. Microelectron Eng. 2008; 85(5–6):1272–4.

45. Ehret R, Baumann W, Brischwein M, Schwinde a, Stegbauer K, Wolf B. Monitoring of cellular behaviour by impedance measurements on interdigitated electrode structures. Biosens Bioelectron. 1997; 12 (1):29–41. PMID: 8976050

46. Süselbeck T, Thielecke H, Weinschenk I, Reininger-Mack A, Stieglitz T, Metz J, et al. In vivo intravascular electric impedance spectroscopy using a new catheter with integrated microelectrodes. Basic Res Cardiol. 2005; 100(1):28–34. https://doi.org/10.1007/s00395-004-0501-8 PMID: 15614589

47. Xu Y, Xie X, Duan Y, Wang L, Cheng Z, Cheng J. A review of impedance measurements of whole cells. Biosens Bioelectron. 2016; 77:824–36. https://doi.org/10.1016/j.bios.2015.10.027 PMID: 26513290

48. Benson K, Cramer S, Galla H-J. Impedance-based cell monitoring: barrier properties and beyond. Fluids Barriers CNS. 2013; 10(1):5. https://doi.org/10.1186/2045-8118-10-5 PMID: 23305242

49. Arndt S, Seebach J, Psathaki K, Galla HJ, Wegener J. Bioelectrical impedance assay to monitor changes in cell shape during apoptosis. Biosens Bioelectron. 2004; 19(6):583–94. PMID: 14683642

50. Wegener J, Seebach J. Experimental tools to monitor the dynamics of endothelial barrier function: A survey of in vitro approaches. Cell Tissue Res. 2014; 355(3):485–514. https://doi.org/10.1007/s00441-014-1810-3 PMID: 24585359

51. Rahman ARA, Register J, Vuppala G, Bhansali S. Cell culture monitoring by impedance mapping using a multielectrode scanning impedance spectroscopy system (CellMap). Physiol Meas. 2008; 29(6).

52. Malleo D, Nevill JT, van Ooyen a, Schnakenberg U, Lee LP, Morgan H. Note: Characterization of electrode materials for dielectric spectroscopy. Rev Sci Instrum. 2010; 81(1):016104. https://doi.org/10.1063/1.3284516 PMID: 20113135

53. Franks W, Schenker I, Schmutz P, Hierlemann A. Impedance characterization and modeling of electrodes for biomedical applications. IEEE Trans Biomed Eng. 2005; 52(7):1295–302. https://doi.org/10.1109/TBME.2005.847523 PMID: 16041993

54. Cote KR, Gill RC. Development of a platinized platinum/iridium electrode for use in vitro. Ann Biomed Eng. 1987; 15(5):419–26. PMID: 3688577

55. Sun T, Swindle EJ, Collins JE, Holloway J a, Davies DE, Morgan H. On-chip epithelial barrier function assays using electrical impedance spectroscopy. Lab Chip. 2010; 10(12):1611–7. https://doi.org/10.1039/c000699h PMID: 20379587

56. Aird WC. Phenotypic Heterogeneity of the Endothelium. Circ Res. 2007; 100(2):158–73. https://doi.org/10.1161/01.RES.0000255691.76142.4a PMID: 17272818

57. Stolwijk JA, Matrougui K, Renken CW, Trebak M. Impedance analysis of GPCR-mediated changes in endothelial barrier function: overview and fundamental considerations for stable and reproducible measurements. Pflügers Arch—Eur J Physiol. 2015; 467(10):2193–218.

58. Wegener J. Impedance analysis of cell junctions. In: Schmid GM, editor. Nanotechnology. Wiley-VCH Verlag GmbH& Co.; 2008. p. 325–57.

59. Wang K, Zhao Y, Chen D, Fan B, Lu Y, Chen L, et al. Specific membrane capacitance, cytoplasm conductivity and instantaneous Young's modulus of single tumour cells. Sci Data. 2017; 4(6):170015.

60. Pethig R, Kell DB. The passive electrical properties of biological systems: their significance in physiology, biophysics and biotechnology. Phys Med Biol. 1987; 32(8):933–70. PMID: 3306721

61. Eker B, Meissner R, Bertsch A, Mehta K, Renaud P. Label-Free Recognition of Drug Resistance via Impedimetric Screening of Breast Cancer Cells. PLoS One. 2013; 8(3):1–12.

62. Stolwijk JA, Michaelis S, Wegener J. Cell Growth and Cell Death Studied by Electric Cell-Substrate Impedance Sensing. In: Jiang WG, editor. Electric Cell-Substrate Impedance Sensing and Cancer Metastasis. Dordrecht: Springer Netherlands; 2013. p. 85–118.

63. Witzel F, Fritsche-Guenther R, Lehmann N, Sieber A, Blüthgen N. Analysis of impedance-based cellular growth assays. Bioinformatics. 2015; 31(16):2705–12. https://doi.org/10.1093/bioinformatics/btv216 PMID: 25900918

64. Dejana E, Corada M, Lampugnani MG. Endothelial cell-to-cell junctions. FASEB J. 1995; 9(10):910–8. PMID: 7615160

65. Kusuma S, Zhao S, Gerecht S. The extracellular matrix is a novel attribute of endothelial progenitors and of hypoxic mature endothelial cells. FASEB J. 2012; 26(12):4925–36. https://doi.org/10.1096/fj.12-209296 PMID: 22919069

66. Rodriguez S, Ollmar S, Waqar M, Rusu A. A Batteryless Sensor ASIC for Implantable Bio-Impedance Applications. IEEE Trans Biomed Circuits Syst. 2016; 10(3):533–44. https://doi.org/10.1109/TBCAS.2015.2456242 PMID: 26372646

67. Iqbal J, Chamberlain J, Francis SE, Gunn J. Role of Animal Models in Coronary Stenting. Ann Biomed Eng. 2016; 44(2):453–65. https://doi.org/10.1007/s10439-015-1414-4 PMID: 26259974

68. Seebach J, Donnert G, Kronstein R, Werth S, Wojciak-Stothard B, Falzarano D, et al. Regulation of endothelial barrier function during flow-induced conversion to an arterial phenotype. Cardiovasc Res. 2007; 75(3):596–607. https://doi.org/10.1016/j.cardiores.2007.04.017 PMID: 17531214

69. Sakamoto N, Kiuchi T, Sato M. Development of an endothelial-smooth muscle cell coculture model using phenotype-controlled smooth muscle cells. Ann Biomed Eng. 2011; 39(11):2750–8. https://doi.org/10.1007/s10439-011-0372-8 PMID: 21811870

70. Truskey G a. Endothelial Cell Vascular Smooth Muscle Cell Co-Culture Assay For High Throughput Screening Assays For Discovery of Anti-Angiogenesis Agents and Other Therapeutic Molecules. Int J High Throughput Screen. 2011; 2010(1):171–81.

71. McKittrick CM, Kennedy S, Oldroyd KG, McGinty S, McCormick C. Modelling the Impact of Atherosclerosis on Drug Release and Distribution from Coronary Stents. Ann Biomed Eng. 2016; 44(2):477–87. https://doi.org/10.1007/s10439-015-1456-7 PMID: 26384667

72. Tsang HG, Rashdan NA, Whitelaw CBA, Corcoran BM, Summers KM, MacRae VE. Large animal models of cardiovascular disease. Cell Biochem Funct. 2016; 34(3):113–32. https://doi.org/10.1002/cbf.3173 PMID: 26914991